JOURNAL OF COMPUTATIONAL PHYSICS 46, 215–236 (1982)

Numerical Solutions of the Traction Problem for a Fibre-Reinforced Material by an Integral-Equation Method

J. A. BELWARD

Department of Mathematics, University of Queensland, St. Lucia, Queensland 4067 Australia

Received October 28, 1981

A method of Atkinson (*Numer. Math.* **10** (1967), 117–124) for solving Fredholm equations of the second kind with nonunique solutions is applied to problems of plane strain/stress of a fibre-reinforced composite. Morland (*Int. J. Solids Struct.* **9** (1973), 1501–1518) has shown that the problem may be reduced to a potential problem with a nonstandard-boundary condition relating pairs of boundary values at the ends of the fibre chords.

Under traction-boundary conditions an integral representation of the displacements leads to an equation with nonunique solutions. A careful examination of the results of Atkinson's method was made and the stress and displacement fields computed for an ellipse under a unidirectional-tensile loading. Plots of the hoop stress are given for a wide range of fibre directions, traction profiles and directions, eccentricities, and material constants.

1. INTRODUCTION

Although the application of integral-equation methods to the numerical solution of boundary value problems has gained increasing prominence lately there remain many types of problems where they are rarely used. One such area is that in which nonuniqueness may occur, as happens with traction problems in the theory of elasticity. A technique developed by Atkinson [1] is available for nonunique solutions so that this should not present a problem.

Morland [2] (and simultaneously England *et al.* [3]) has set up a model for fibre-reinforced materials based on classical-infinitesimal theory with an assumption of inextensibility in the fibre directions. In problems of plane strain or plane stress in which the fibres are parallel, the displacement perpendicular to the fibre directions is shown to be a harmonic function. The pure traction problem involves a nonstandard-boundary condition and is ideally suited to an integral-equation method. Since the displacements are only determined to within a rigid-body rotation there is a nonuniqueness to be taken into account.

In a subsequent paper Morland [4] proved the existence of solutions of the problem but the construction of solutions is not possible by analytic methods, thus a

0021-9991/82/050215-22$02.00/0

numerical approach is needed. The purpose of this work is to demonstrate the effectiveness of the method of Atkinson and to present a numerical solution of the boundary value problem.

Procedures for the reduction of potential problems in two and three dimensions to integral equations are readily available in the literature (see [5], e.g.) and Fredholm equations of the first or second kind may be constructed. Normally the latter type present fewer numerical problems. Techniques for equations of the second kind are reviewed by Atkinson [6]; broadly speaking two classes of methods can be identified, quadrature methods and expansion methods. Atkinson's technique for dealing with nonuniqueness may be used with either method. In the current work a Nystrom method was used; this combines a quadrature method with collocation. The kernel of the integral equation constructed was logarithmically singular, it is easily dealt with by the use of a product-integration quadrature rule, i.e., one in which the singularity is included by writing the integral as a product of the singular part and some suitable approximant.

Many practical uses have been found for fibre-reinforced composites lately and this has stimulated the formulation of simple models of these materials in continuum mechanics. In a recent article Pipkin [7] has given an account of developments of both the finite and infinitesimal theories over the last decade. The model developed by Morland is valid for a variety of geometries, finite or infinite, convex or nonconvex. The results to be given in this paper concern an elliptical domain whose axes of symmetry are oriented at an arbitrary angle to the fibre direction. A unidirectional tension was applied with the direction of action at a further arbitrary angle to the semi axes. Profiles of the distributed tension were varied between peaked and near-flat shapes. Plots of the hoop stress against eccentric angle are given for a wide range of material constants and eccentricities.

The numerical method worked well, certainly well enough to enable some exact relations to be discovered. Working in single-precision arithmetic with a relative-machine precision of 5×10^{-8}, six digits of accuracy were normally obtained.

In order to apply Atkinson's method the eigensystem of the kernel and its transpose at the eigenvalue in question must be determined. As the computing progressed, enough evidence was accumulated to enable the eigenfunctions to be verified analytically. The availability of the exact eigensystem enabled a suitable level of discretisation to be chosen. The nonuniqueness is overcome by a device which implicitly selects one of the multiplicity of solutions of the integral equation. The analysis predicts that the exact solution selected will be zero at certain of the collocation points. This provides a valuable guide to the accuracy of the approximate solution. Solutions only exist when the prescribed function of the integral equation is orthogonal to the eigenfunctions of the transposed kernel. In determining a suitable family of loading functions it was shown that this abstract condition is equivalent to the requirements of zero-net force and zero net-turning moment on the ellipse.

The stresses are calculated by differentiating the displacement fields. The level of noise due to rounding and discretisation was sufficiently low as to enable the derivatives to be determined from the derivative of the sixth-degree polynomial inter-

polant centred on the point in question. Exact solutions for one particular set of traction profiles were discovered from the numerical results, thus it was possible to check the entire procedure.

The results are given in Section 6. Values of the hoop stress were of more or less constant magnitudes within the parameter ranges used. As the orientation of the fibre lines was changed the response as measured by the hoop stress was not as varied as anticipated. The eccentricity was the most sensitive parameter. As $e \to 1$, when the ellipse becomes more slender, the slopes and curvature of the plots become much greater and the computation required increasingly higher discretisation levels to maintain accuracy.

The results obtained are regarded as good enough to merit further use of the technique. Further numerical experiments would be of value and a comparison with methods based on more established methods would be of interest.

The paper is set out as follows. In Section 2 Morland's work is summarised in sufficient detail to outline the setting up of the boundary value problem. Formulation of the integral equation is made in Section 3, where the role of the abstract orthogonality relations are shown to be equivalent to the equilibrium conditions. In Section 4 we shall focus on the particular case of an ellipse and derive a condition which enables simple identification of the admissible unidirectional tension profiles. Atkinson's method, the Nystrom method and their applications to the current problem are explained in Section 5. The final section contains a description of the results of the computation.

2. Mathematical Description of the Problem

In this section the derivation of the mathematical description of the problem is summarised. A more detailed account of the basic properties of inextensible transversely isotropic composites is given by Morland in [2].

The presence of the fibres renders the material inextensible in the fibre direction and transversely isotropic and problems are considered in which linear-elasticity theory is assumed valid. Let u, v, and w be the displacements referred to a Cartesian $0xyz$ system with the fibre direction parallel to the x axis.

In problems of plane strain or plane stress, inextensibility implies that

$$\frac{\partial u}{\partial x} = 0 \Rightarrow u = u(y), \tag{2.1}$$

and it follows from the stress–strain relations that

$$\sigma_{yy} = \frac{\mu_L}{c^2}\frac{\partial v}{\partial y}, \qquad \sigma_{xy} = \mu_L\left(\frac{\partial v}{\partial x} + \frac{\partial u}{\partial y}\right), \tag{2.2a, b}$$

where μ_L is the shear modulus in the x direction and c is given by

$$c^2 = \frac{\mu_L}{k_T + \mu_T} \qquad \text{or} \qquad c^2 = \frac{\mu_L(k_T + \mu_T)}{4\mu_T k_T} \tag{2.3a, b}$$

for plane strain or stress, respectively. The shear modulus μ_T is perpendicular to the x direction and k_T is the bulk modulus for plane strain in the transverse, yz plane.

In the absence of body forces the y component of the equilibrium equations becomes

$$c^2 \frac{\partial^2 v}{\partial x^2} + \frac{\partial^2 v}{\partial y^2} = 0 \tag{2.4}$$

while the x component may be integrated to give

$$\sigma_{xx} = -\mu_L \left(x u''(y) + \frac{\partial v}{\partial y} \right) + t(y). \tag{2.5}$$

In the last equation $t(y)$, which appears as an arbitrary function of integration, is determined by the equilibrium conditions at the boundary.

For convenience the scaled coordinates

$$X = x \qquad \text{and} \qquad Y = cy \tag{2.6}$$

are introduced and corresponding quantities in this system denoted by capitals, thus $v(X, Y/c) = V(X, Y)$.

V is thus harmonic, viz.

$$\frac{\partial^2 V}{\partial X^2} + \frac{\partial^2 V}{\partial Y^2} = 0 \tag{2.7}$$

and it is shown below that in the case of a pure traction problem a boundary condition on V can be set up in terms of the prescribed tractions. Once V is determined the values of U and $\boldsymbol{\sigma}$ are easily calculated from equations (2.2), (2.5), and (2.10). In the present work we shall consider finite domains convex to the fibre lines; more general configurations and boundary conditions are treated in [2] and [4].

The boundary condition on V is found as follows: If $\mu_L t_x$ denotes the x component of traction, then the integral of this quantity around ∂D may be combined with Eqs. (2.2a) and (2.5) to give

$$V + cXU'(Y) = M(S) + J(Y), \tag{2.8}$$

where

$$J(Y) = \frac{1}{c} \int_{Y_B}^{Y} T(Y')\, dY' \quad \text{and} \quad M(S) = \frac{\mu_L}{c} \int_0^S (\cos^2 \phi + c^2 \sin^2 \phi)^{1/2}\, t_x\, dS'. \tag{2.9a, b}$$

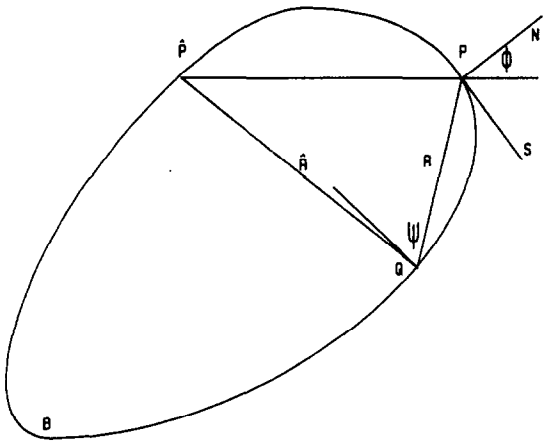

FIGURE 2.1

Figure 2.1 is used to define S, ϕ, and any further variables associated with the geometry of D. S is measured from B, the minimum point for Y on ∂D. The y component of the equilibrium equations when written in terms of the scaled coordinates becomes

$$\frac{\partial V}{\partial N} + c\cos\phi U'(Y) = (\cos^2\phi + c^2\sin^2\phi)^{1/2}\mu_L t_y = L(S), \tag{2.10}$$

($\mu_L t_y$ is the y component of the traction on ∂D).

Now if (X, Y) and $(\hat{X}, Y)$ are the ends of a fibre chord and $\hat{V}$ denotes $V(\hat{X}, Y)$, by applying (2.8) and (2.9) at both (X, Y) and $(\hat{X}, Y)$, J and U' may be eliminated to give the single condition for V

$$\frac{\partial V}{\partial N} - \frac{\cos\phi}{X-\hat{X}}(V-\hat{V}) = L - \frac{\cos\phi}{X-\hat{X}}(M-\hat{M}) \qquad \text{on } \partial D. \tag{2.11}$$

In the traction problem $L(S)$ and $M(S)$ are prescribed functions.

If the domain D is symmetric about a normal to the fibre lines the problem may be simplified to a Neumann problem and a Robin problem (Morland [2]), thus in what follows we shall be concerned with domains oriented asymmetrically with respect to the fibre lines and we shall solve Eq. (2.7) subject to boundary condition (2.11).

3. THE INTEGRAL EQUATION

The boundary value problem described by Eqs. (2.7) and (2.11) may be reformulated as an integral equation. This is set up using the standard results on representations of harmonic functions. Since the basic model admits nontrivial solutions

which represent rigid body motions for zero boundary tractions, the integral equation will have homogeneous solutions which generate these displacement fields. The integral operators generated by the representations of the harmonic function V are compact and thus the Fredholm alternative applies to the integral equation derived. The eigensystems of the kernel and the transpose are given below where it is also shown that the orthogonality conditions (on the prescribed function g, defined at (3.4)) of the Fredholm theory are equivalent to the equilibrium conditions on the boundary tractions.

Many representations of V are possible, here we take

$$V(P) = \int_{\partial D} f(S') \log R \, dS' \tag{3.1}$$

(see Fig. 2.1 for the notation), then by standard potential theory

$$\frac{\partial V}{\partial N} = -\pi f(S) + \int_{\partial D} f(S') \frac{\cos \psi}{R} \, dS'. \tag{3.2}$$

Thus f satisfies the integral equation

$$-\pi f(S) + \int_{\partial D} f(S') \left[\frac{\cos \psi}{R} - \frac{\cos \phi}{X - \hat{X}} \log \left(\frac{R}{\hat{R}} \right) \right] dS' = g(S), \tag{3.3}$$

where

$$g(S) = L(S) - \frac{\cos \phi}{X - \hat{X}} (M(S) - M(\hat{S})). \tag{3.4}$$

It is shown in [4] that for zero data there is a solution

$$V = V_0 + V_1 X, \qquad U = U_0 - V_1 Y/c \tag{3.5a, b}$$

for arbitrary values of U_0, V_0, and V_1. Thus Eq. (3.3) has an eigenvalue equal to π with null space of dimension 2. Implementation of the numerical scheme described in Section 5 requires the eigensystems of K and its transpose K^*. Whilst these may be determined numerically, analytical expressions are clearly preferable. In the following paragraphs we determine these analytical expressions.

Evidently $f(S) = 1$ is one eigenfunction, for if $V = 1$, then $f(S)$ satisfies

$$\pi f(s) = \int_{\partial D} f(S') \frac{\cos \psi}{R} \, dS' \tag{3.6}$$

and this equation has $f(S) = 1$ as its only solution (Jaswon and Symm, [5, Chap. 3]).

For $V = X$ Eqs. (3.1) or (3.2) may be regarded as an equation for f. An analytical solution is not available for arbitrary contours, however, when D is an ellipse, the

solution can be given. In terms of the parameterisation described in detail in the next section, we have

$$f(S) = \cos(\lambda + \alpha), \tag{3.7}$$

where λ is the eccentric angle and α is the angle between the fibre lines and the major axis of the ellipse (cf. Fig. 4.1).

The transposed kernel differs only slightly from the original kernel, the singular part being symmetric, thus it is natural to guess $f(S) = 1$ again, and this is easily verified by direct calculation. It is clear that the second eigenfunction is X. While a rigorous proof cannot be given, it can be shown that the equilibrium conditions imply that X is orthogonal to $g(S)$ and the numerical evidence in support of the assertion is overwhelming (see the results in Section 6(ii)).

If 1 and X are the eigenfunctions of the transpose then

$$\int_{\partial D} g(S')\, dS' = 0 \qquad \text{and} \qquad \int_{\partial D} X' g(S')\, dS' = 0, \tag{3.8a, b}$$

and it may be shown that these are implied by the equilibrium conditions as follows: Taking the left-hand side of Eq. (3.8a) and using the relationships (3.4), (2.9b), and (2.10) we have

$$\int_{\partial D} g(S')\, dS' = \int_{\partial D} \left(L - \frac{\cos\phi}{X - \hat{X}} (M - \hat{M}) \right) dS'. \tag{3.9}$$

If the first term on the right-hand side of (3.9) is written in unscaled variables it becomes

$$\int_{\partial D_i} t_y\, ds$$

and is the total force on D_i (the domain D referred to the unscaled system) in the y direction. For the second term on the right of (3.9), the integral which defines M may also be written in unscaled coordinates and identified as the integrated x component of the applied force on the boundary. This will thus be single valued on ∂D if and only if the total force in the x direction is zero. Thus we may write the second integral on the right of (3.9) as the integral along the left- and right-hand side of ∂D. The variable of integration may then be changed to Y and we obtain

$$\int_{\partial D} \cos\phi \frac{M - \hat{M}}{X - \hat{X}}\, dS = \int_{Y_B}^{Y_T} \frac{M_L - M_R}{X_L - X_R}\, dY' + \int_{Y_T}^{Y_B} \frac{M_R - M_L}{X_R - X_L}\, dY' = 0. \tag{3.10}$$

Thus it has been shown that the zero net-force condition implies that the right-hand

side of (3.9) is zero and hence that (3.8a) is satisfied. Next consider the left-hand side of Eq. (3.8b); it may be expressed as

$$\int_{\partial D} X'g(S')\,dS' = \int_{\partial D} X' \left(L' - \frac{\cos\phi'}{X' - \hat{X}}(M' - \hat{M}')\right) dS'. \tag{3.11}$$

Now the integral expression which equals the total turning moment may be transformed to scaled (X, Y) coordinates and each term integrated by parts so that

$$\int_{\partial D_i} (xt_y - yt_x)\,ds = \int_{\partial D} (XL - M\cos\phi)\,dS. \tag{3.12}$$

The right-hand sides of (3.11) and (3.12) will be equal if

$$\int_{\partial D} \cos\phi \frac{(M\hat{X} - X\hat{M})}{X - \hat{X}}\,dS = 0. \tag{3.13}$$

The same argument which was used to obtain (3.10) may be applied again. Thus through Eq. (3.13) we see that the zero total-turning moment condition implies Eq. (3.8b).

4. The Traction Problem for an Ellipse

While the methods and analyses used in this work are applicable to any convex domain it is preferable at this point to select a particular domain D. Symmetry about an axis perpendicular to the fibre lines is excluded since this leads to standard potential problems, thus an ellipse having its axes of symmetry at an arbitrary angle to the fibre lines was chosen. Some details concerning the parameterisation of D are given below followed by the derivation of the important relationship (4.15). This relationship facilitates a choice of traction profiles for which the zero turning-moment condition (and equivalently the eigenfunction conditions on the prescribed function for the integral equation) is satisfied. It also transpires that several superficially distinct problems lead to one particular right-hand side.

The ellipse has its major axis at an angle α to the fibre direction, the lengths of its semi-axes are a and b, and λ parameterises the perimeter. Figure 4.1 shows further details.

It is convenient to express

$$X = X_E \cos(\lambda - \lambda_E), \qquad Y = Y_T \cos(\lambda - \lambda_T), \tag{4.1}$$

where

$$X_E = (a^2\cos^2\alpha + b^2\sin^2\alpha)^{1/2}, \qquad Y_T = (a^2\sin^2\alpha + b^2\cos^2\alpha)^{1/2}. \tag{4.2}$$

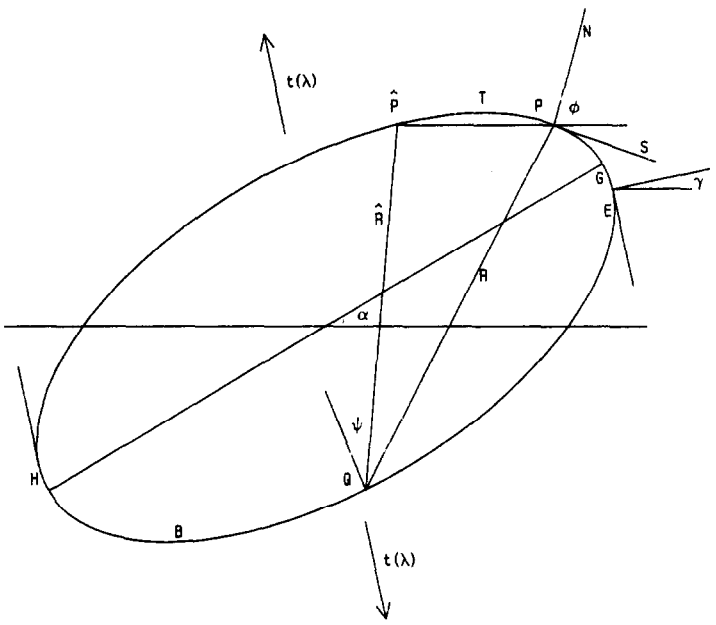

FIGURE 4.1

We also have

$$\lambda + \hat{\lambda} = 2\lambda_T, \tag{4.3}$$

$$\cos\phi = \frac{-Y_T \sin(\lambda - \lambda_T)}{(a^2 \sin^2\lambda + b^2 \cos^2\lambda)^{1/2}}, \quad \text{and} \quad X - \hat{X} = 2X_E \sin(\lambda_E - \lambda_T)\sin(\lambda - \lambda_T). \tag{4.4}$$

If the eccentric angles at P and Q are λ and μ,

$$R^2 = 4\sin^2((\lambda-\mu)/2)(a^2\sin^2((\lambda+\mu)/2) + b^2\cos^2((\lambda+\mu)/2)), \tag{4.5}$$

and

$$\cos\psi/R = ab/2(a^2\sin^2\mu + b^2\cos^2\mu)^{1/2}\,(a^2\sin^2((\lambda+\mu)/2) + b^2\cos^2((\lambda+\mu)/2)). \tag{4.6}$$

On substituting these expressions into Eq. (3.3) and expressing

$$\begin{aligned} F(\lambda) &= \pi f(\lambda)(a^2\sin^2\lambda + b^2\cos^2\lambda)^{1/2}, \\ G(\lambda) &= g(\lambda)(a^2\sin^2\lambda + b^2\cos^2\lambda)^{1/2} \end{aligned} \tag{4.7}$$

we obtain

$$\int_0^{2\pi} F(\mu)\, K(\lambda, \mu)\, d\mu - F(\lambda) = G(\lambda), \tag{4.8}$$

where

$$2\pi K(\lambda,\mu) = \frac{ab}{(a^2 \sin^2((\lambda+\mu)/2) + b^2 \cos^2((\lambda+\mu)/2))} + \frac{Y_E}{X_T \sin(\lambda_E - \lambda_T)}$$
$$\times \log\left(\frac{\sin^2((\lambda-\mu)/2)(a^2 \sin^2((\lambda+\mu)/2) + b^2 \cos^2((\lambda+\mu)/2))}{\sin^2(\lambda_T - ((\lambda+\mu)/2))(a^2 \sin^2(\lambda_T - (\lambda/2) + (\mu/2)) + b^2 \cos^2(\lambda_T - (\lambda/2) + (\mu/2)))}\right). \tag{4.9}$$

The singular part of $K(\lambda, \mu)$ is

$$K^{(s)}(\lambda,\mu) = \frac{(2\pi)^{-1} Y_E}{X_T \sin(\lambda_E - \lambda_T)} \log\left[\frac{\sin^2((\lambda-\mu)/2)}{\sin^2((2\lambda_T - \lambda - \mu)/2)}\right]$$

with singularities at the zeros of the sine functions. Since $0 \leqslant \lambda,\ \mu \leqslant 2\pi$, and $0 \leqslant \lambda_T \leqslant \pi$, these are on the lines $\lambda - \mu = 0$, $\lambda = 2\lambda_T - \mu$, $\lambda = 2\lambda_T - \mu + 2\pi$, and at points $\lambda = 0$, $\mu = 2\pi$ and $\mu = 0$, $\lambda = 2\pi$. The regular part of $K(\lambda, \mu)$ is C^∞.

The function $G(\lambda)$ is determined by combining Eqs. (2.9a), (2.10), (3.4), and (4.7b). The loadings which have been investigated are unidirectional tensions with several different profiles, and a hydrostatic-pressure loading. As mentioned earlier several apparently different problems lead to the same $G(\lambda)$. To identify these first suppose the tension acts perpendicular to the fibre lines, then $t_x = 0$, and by applying the same forces on opposite sides of the ellipse the zero net-force condition is satisfied. For this special case the zero-moment condition (3.8b) can be written

$$\int_{\lambda_E}^{\lambda_E + 2\pi} t_y \cos(\lambda - \lambda_E)(c^2 \sin^2\phi + \cos^2\phi)^{1/2} (a^2 \sin^2\lambda + b^2 \cos^2\lambda)^{1/2}\, d\lambda = 0, \tag{4.10}$$

thus we may take

$$t_y = r(\lambda)(c^2 \sin^2\phi + \cos^2\phi)^{-1/2} (a^2 \sin^2\lambda + b^2 \cos^2\lambda)^{-1/2}, \tag{4.11}$$

for any $r(\lambda)$ orthogonal to $\cos(\lambda - \lambda_E)$. The square-root factors arise from changing the variable of integration and in the original (x, y) system t_y varies as $\sin(\lambda - \lambda_E)$. An obvious choice is $r(\lambda) = \sin(\lambda - \lambda_E)$, and in this case G and r are identical, thus

$$G(\lambda) = \sin(\lambda - \lambda_E). \tag{4.12}$$

A second special case is that of a hydrostatic pressure p applied to ∂D_i. Then if θ is the angle of direction of the normal,

$$t_y = -p \sin\theta, \qquad t_x = -p \cos\theta. \tag{4.13}$$

Upon transforming the θ dependence we obtain

$$t_y = -pX_E \sin(\lambda - \lambda_E)(c^2 \sin^2 \phi + \cos^2 \phi)^{-1/2} (a^2 \sin^2 \lambda + b^2 \cos^2 \lambda)^{-1/2}$$

while t_x into Eq. (2.9b) gives $M = \hat{M}$ for any point. Thus $G(\lambda)$ is again, apart from a constant multiplier, given by (4.12).

In the general case suppose a tension $t(\lambda)$ is applied parallel to the tangents at G and H as indicated in Fig. 4.1. The turning moment on the ellipse evaluated in scaled coordinates is

$$N = \int_{\partial D} (X \cos \gamma + Y \sin \gamma)(c^2 \sin^2 \gamma + \cos^2 \gamma)^{-1/2} t(\lambda)\, dS' \tag{4.14}$$

which in terms of λ becomes

$$N = k \int_{\beta}^{\beta + 2\pi} \cos(\lambda - \beta)\, t(\lambda)(c^2 \sin^2 \phi + \cos^2 \phi)^{1/2} \times (a^2 \sin^2 \lambda + b^2 \cos^2 \lambda)^{1/2}\, d\lambda, \tag{4.15}$$

where k depends on α, β, γ, etc. and β is the value of λ at G. Thus we may choose any $t(\lambda)$ orthogonal to

$$\cos(\lambda - \beta)(c^2 \sin^2 \phi + \cos^2 \phi)^{1/2} (a^2 \sin^2 \lambda + b^2 \cos^2 \lambda)^{1/2}. \tag{4.16}$$

Finally note that by choosing

$$t(\lambda) = \sin(\lambda - \beta)(c^2 \sin^2 \phi + \cos^2 \phi)^{-1/2} (a^2 \sin^2 \lambda + b^2 \cos^2 \lambda)^{-1/2}, \tag{4.17}$$

although $M - \hat{M}$ does not vanish pointwise, after a lengthy manipulation we obtain a $G(\lambda)$ proportional to $\sin(\lambda - \lambda_E)$. Hence $G(\lambda)$ serves for three examples, the first being a particular case of the last. Note, however, that only one field variable V is the same in all three problems, since different data will be used in the equations which determine U and σ.

In the next two sections some further choices of $t(\lambda)$ will be described.

5. Description of the Numerical Solution of the Integral Equation

The numerical procedure has two parts, first an equivalent equation is constructed which has a unique solution and then the new equation is discretised to obtain a finite-linear system. The former task offers the greater difficulty and was dealt with by using a technique developed by Atkinson [1]. Although the method appears to have attracted little attention (except for Baker [8]) it is easy to use and gave good results on the current problem. Discretisation of the eqution requires a product-integration rule to take account of the logarithmic singularities in the kernel but is

otherwise straightforward. A formal description of Atkinson's method is given below and [1] should be consulted for the precise analytical details.

Let the integral equation be given on $[a, b]$ and denoted by

$$(\Lambda - K) F = G, \tag{5.1}$$

where Λ is a scalar and K the compact operator generated by the kernel on the space of continuous functions $C[a, b]$ with sup norm. F and G belong to $C[a, b]$. Suppose there are m linearly independent eigenfunctions of K, $\theta_1, \theta_2, \ldots, \theta_m$, say, corresponding [illegible] transpose of K by $\theta_1^*, \ldots, \theta_m^*$.

A linear operator L is defined by

$$LF(\lambda) \equiv \sum_{k=1}^{m} F(\mu_k)\, \theta_k^*(\lambda), \tag{5.2}$$

$(a \leqslant \mu_1 < \mu_2 < \cdots < \mu_k \leqslant b)$ and Eq. (5.1) is replaced by

$$(\Lambda - K - L) F = G. \tag{5.3}$$

It is shown in [1] that provided

$$\det \theta_i(\mu_j) \neq 0, \tag{5.4}$$

$(\Lambda - K - L)^{-1}$ exists on $C[a, b]$ and further when G belongs to the range of $(\Lambda - K)$ the solution of Eq. (5.3) simultaneously satisfies

$$(\Lambda - K) F = G \qquad \text{and} \qquad LF = 0. \tag{5.5a, b}$$

Since the eigenfunctions θ_k^* are independent (5.5b) implies that $F(\mu_k) = 0$ for each μ_k. Thus we solve Eq. (5.3) instead of Eq. (5.1), the values of $F(\mu_k)$ are treated as unknowns and when G belongs to the range of $(\Lambda - K)$ they should be found to be zero. Note that the definition of L contains an arbitrariness (because *any* spanning set $\{\theta_k^*\}$ may be chosen) which is analytically irrelevant, but may be important in a numerical approximation scheme. This point is taken up in Section 6(iii).

Approximate solutions of Eq. (5.3) were found using a Nystrom scheme. For a conventional-integral equation with a continuous kernel this entails approximation of the integral operator by a quadrature rule followed by collocation at the quadrature points. In the current problem the presence of the operator L necessitates the introduction of extra collocation points and the singularities in the kernel need special treatment in the approximation of K in order to ensure a reasonable rate of convergence.

In order to approximate K the kernel is written as the sum of its regular and singular parts $K^{(R)}(\lambda, \mu)$ and $K^{(S)}(\lambda, \mu)$, respectively, then

$$\int_a^b K(\lambda, \mu)\, F(\mu)\, d\mu = \int_a^b K^{(R)}(\lambda, \mu)\, F(\mu)\, d\mu + \int_a^b K^{(S)}(\lambda, \mu)\, d\mu. \tag{5.6}$$

Each term on the right-hand side of (5.6) was approximated using a piecewise-quadratic approximant. For the first integral Simpson's rule was applied to the integrand $F(\mu)\,K^{(R)}(\lambda,\mu)$ while for the second term the quadratic which interpolates $F(\mu_{2j})$, $F(\mu_{2j+1})$, $F(\mu_{2j+2})$ was integrated up exactly with $K^{(S)}(\lambda,\mu)$, thus we express

$$\int_a^b K(\lambda,\mu)\,F(\mu)\,d\mu \cong \sum_{j=1}^{n} (w_j K^{(R)}(\lambda,\mu_j) + k_j^{(S)}(\lambda)\,F(\mu_j)), \tag{5.7}$$

where w_j are the weights for Simpson's rule and $k_j^{(S)}(\lambda)$ are the singular weights obtained as explained above.

Equation (5.3) is then approximated by

$$\begin{aligned} &\lambda F_n(\lambda) - \sum_{j=1}^{n} (w_j K^{(R)}(\lambda,\mu_j) + k_j^{(S)}(\lambda))\,F_n(\mu_j) \\ &\quad - \sum_{k=1}^{m} F_n(\nu_k)\,\theta_k^*(\lambda) = G(\lambda). \end{aligned} \tag{5.8}$$

(The notation distinguishes between F_n the solution of (5.8) and F the solution of (5.2).) Approximate solutions of this equation are determined by satisfying Eq. (5.8) at the points $\lambda = \mu_1, \mu_2, \ldots, \mu_n, \nu_1, \ldots, \nu_m$, thereby obtaining an $(n+m)\times(n+m)$ system viz.

$$\begin{bmatrix} \lambda I_n - A_n & -B_n \\ -C_n & \lambda I_m - D_n \end{bmatrix} \begin{bmatrix} \mathbf{F}_n^{(1)} \\ \mathbf{F}_n^{(2)} \end{bmatrix} = \begin{bmatrix} \mathbf{G}^{(1)} \\ \mathbf{G}^{(2)} \end{bmatrix} \tag{5.9}$$

in which I_n, I_m are unit matrices of order n and m, respectively, and

A_n	is	$n \times n$	and	$a_{ij} = k_j^{(S)}(\lambda_i) + w_j K^{(R)}(\lambda_i,\mu_j)$,
B_n	is	$n \times m$	and	$b_{ij} = \theta_j^*(\lambda_i)$,
C_n	is	$m \times n$	and	$c_{ij} = k_j^{(S)}(\nu_i) + w_j K^{(R)}(\nu_i,\mu_j)$,
D_n	is	$m \times m$	and	$d_{ij} = -\theta_j^*(\nu_i)$.

$\mathbf{G}^{(1)}$, $\mathbf{G}^{(2)}$ are the vectors of values of G at $\mu_1, \ldots, \mu_n$, $\nu_1, \ldots, \nu_m$, and $\mathbf{F}_n^{(1)}$, $\mathbf{F}_n^{(2)}$ are the vectors of approximate values of F at these points. In the case when Eq. (5.1) has a unique solution B_n, C_n and D_n are absent, and if the kernel were continuous $k^{(S)}(\lambda)$ would not appear.

It may be shown (Atkinson [6]) that if F is four times continuously differentiable, then

$$\|F - F_n\|_\infty = O(h^4 \log h) \tag{5.10}$$

(where $nh = b - a$).

6. Results

In this section the results of the numerical method are given; for ease of presentation the description is divided into 6 subsections. All computations quoted below were carried out in single precision arithmetic on a DEC PDP 10 at the University of Queensland which has a 27 bit binary mantissa; relative machine precision is thus $1 \times 10^{-8.4}$.

(i) *Parameter Values and Loading Profiles*

Before the results are given in detail the range of parameter values will be discussed. Since the applied tractions form part of the input data these are also given.

The physical model contains two material parameters, the constants c and μ_L which appear in Eqs. (2.2) and (2.3). In traction problems the constant μ_L can be absorbed into the prescribed loadings and their magnitudes factored by μ_L, leaving c as the remaining parameter. For c the range $0.5 \leqslant c \leqslant 1$ was used, this being the range of values suggested by experimental data (Morland [2]).

The geometry of the problem gives rise to further parameters, namely, the angle of orientation of the fibre chords and the eccentricity of the ellipse. Values of the eccentricity from 0.6 upwards were used, generally to 0.968, the latter value corresponding to a minor/major axis ratio of 0.25. Values above 0.968 are tractable but as the eccentricity approaches unity the rate of convergence is reduced and the computation becomes more susceptible to rounding error.

Certain parameters are associated with the traction profiles. When a unidirectional tension is applied to opposite sides of the ellipse both the direction of the tension and the tension profile may vary. Solutions were computed for a full range of tension directions and sets of profiles from sharply peaked to flat, near-uniform distributions. A uniform-circumferential pressure was also investigated.

(ii) *Discretisation and the Eigensystem of the Coefficient Matrix A_n*

In order to apply Atkinson's method the eigenfunctions of the integral operators K and K^* corresponding to $\Lambda = 1$ are required. Numerical results obtained in early programme development provided the stimulus for the analytical derivation of the eigensystems outlined in Sections 3 and 4. These theoretical results in turn provided valuable information on the accuracy of the discretisation.

It was observed that the best accuracy was obtained by integrating from $\lambda_T - \pi$ to $\lambda_T + \pi$. This may be anticipated, for relation (4.3) ensures that if λ_j is a quadrature point, so too is $\hat{\lambda}_j$, provided λ_T is itself a quadrature point. When this happens the approximate values for the integrals of $\log R$ and $\log \hat{R}$ corresponding to $f(S) = 1$ balance exactly, leaving only the regular part to be approximated.

The eigensystem of A_n approximates that of K. Since unity is a once repeated eigenvalue of K there should be two eigenvalues of A_n which are perturbations of unity. These were computed for values of n from 16 to 64, α between 0.05236 ($= 3°$) and 1.4835 ($= 85°$) and the eccentricity from 0.6 up to 1.0. Fixing α and e first at 0.87266 ($= 50°$) and 0.866, respectively, for $n = 16$ the two largest roots differ from

unity by 3×10^{-5} and 4×10^{-4} and the next largest root is about 0.7. As n increases up to 64 these differences reduce steadily to 1×10^{-7} and 2×10^{-7}, the former being 1 decimal digit in the eighth position and thus attributable to rounding error. With n set equal to 32 and e fixed at 0.866, the values of α were found to have little influence on the results, thus at $\alpha = 0.05236$, perturbations from unity were 1×10^{-7} and 2×10^{-5} with next largest magnitude root about -0.3 while at $\alpha = 1.4835$ the perturbations were 1×10^{-7} and 5×10^{-5} with next largest root at 0.7.

The values of the eccentricity have a much greater influence. With $n = 32$ and $\alpha = 0.87266$, values of e below 0.866 gave progressively better results as e was reduced, and as e gets nearer unity the perturbations increase. The larger perturbation for $e = 0.943$, 0.968 and 0.990 were, respectively, 3×10^{-5}, 6×10^{-5}, and 2×10^{-3}, and the third eigenvalue increased from 0.77 to 0.98. A run with $e = 0.999$ gave 8 of the 33 roots near 0.93, the closest to unity being 0.936. The ratio of the lengths of the minor to major axis is about $\frac{1}{4}$ for $e = 0.968$, if $e = 0.990$ the ratio is $\frac{1}{7}$, and at this point some approximation of the physical model should be used to take the slender shape into account.

Accurate results for the eigenvalues need not guarantee good approximations to the eigenfunctions. The accuracy of the eigenfunctions was measured by evaluating the Euclidean distance of each of the computed eigenvectors from the space spanned by the exact eigenvectors (*exact eigenvector* means the vector of values of the exact eigenfunctions at the quadrature points). The projection of the computed eigenvectors onto the exact eigenspace was also calculated and compared componentwise with the computed eigenvector. In Table 6.1 we have tabulated the quantities

$$d_i^2 = \min_{\alpha,\beta} \| \theta_i^{(c)} - \alpha_i \theta_1^{(e)} - \beta_i \theta_2^{(e)} \|_2^2 \tag{6.1}$$

$$f_i = \| \theta_i^{(c)} - a_i \theta_1^{(e)} - b_i \theta_2^{(e)} \|_\infty \tag{6.2}$$

for $i = 1$ and 2, with $\theta_i^{(c)}$ and $\theta_i^{(e)}$ the computed and exact eigenvectors normalised to length unity, a_i and b_i being the minimising values of α_i and β_i. The results confirm

TABLE 6.1

Pointwise and Mean-Square Distances of the Computed Eigenfunctions from the Exact Eigenspace

$\alpha = 0.87266$		$e = 0.866$			$\alpha = 0.87266$		$e = 0.968$	
d_1^2	d_2^2	f_1	f_2	n	d_1^2	d_2^2	f_1	f_2
2(−8)	6(−8)	3(−5)	1(−4)	16	4(−4)	1(−4)	7(−3)	3(−3)
4(−9)†	5(−8)	3(−7)	3(−6)	32	3(−8)	5(−8)	3(−5)	7(−5)
2(−9)†	−6(−9)†	4(−7)	4(−8)	64	1(−9)†	8(−6)	5(−7)	2(−6)

† These are zero to machine precision, $a(-b)$ means $a \times 10^{-b}$.

TABLE 6.2

Approximate Eigenvalues of the Kernel and Its Transpose

$\alpha = 0.87266$ $e = 0.866$	$n = 16$		$n = 32$	
Kernel	1.0000339	0.99961522	1.0000002	0.99997419
Transpose	1.0000339	0.99962537	1.0000002	0.99997423

the analytic derivation of the eigenfunctions of Section 4. They also show that the dependence of the discretisation errors on n and e is very similar for both the eigenvalues and eigenvectors.

The same exercise carried out on the transposed kernel gave almost identical results. In Table 6.2 the computed eigenvalues (near unity) of the kernel and its transpose are compared. On the basis of these results most further computations were made with $n = 32$.

(iii) *Solutions of the Integral Equation*

After checking the eigensystem of the matrix A_n, the left-hand side of Eq. (5.9) was set up. The submatrix $[B_n \vdots D_n]^T$ consists of two columns of values of two independent eigenfunctions of the transposed kernel. The constant and cosine eigenfunctions were used. The columns of this submatrix were chosen to have Euclidean norm equal to unity, and the ∞, 2, and 1 norms were calculated for each column of the whole matrix. These were all within the same order of magnitude and were therefore accepted as suitable. Note, as observed in Section 5, that theoretically any multiple of either column is as equally acceptable as any other.

In general an explicit expression for $G(\lambda)$ was not derived and the right-hand side of Eq. (5.9), $[\mathbf{G}^{(1)} \vdots \mathbf{G}^{(2)}]^T$ was determined by prescribing $t(\lambda)$, the tension profile, and

[illegible] $G(\lambda)$ reduces to a manageable analytic expression.)

Since the theory predicts that $F(v_i) = 0$ this provides a useful check on the solutions. The two values of $F_n(v_i)$ and the value of the maximum of $|F_n(\mu_i)|$ are

TABLE 6.3

Values of the Solution of the Integral Equation at the Extra Collocation Points

Function	t_1	t_2	t_3	t_4
$F_n(v_1)$	−3.3(−9)	−1.4(−8)	−1.9(−8)	1.5(−9)
$F_n(v_2)$	−7.4(−6)	−1.4(−5)	−1.9(−5)	4.2(−6)
$\|F_n(\mu_i)\|_\infty$	1.7(−1)	3.3(−1)	4.6(−1)	1.9(−1)

compared in Table 6.3 and give a good verification of the theory. The functions used for the right-hand sides correspond to the loadings

$$t_1(\lambda) = \frac{d\lambda}{ds}(1/2\mu_L)\sin(\lambda - \beta), \tag{6.3a}$$

$$t_2(\lambda) = \frac{d\lambda}{ds}\frac{3}{4\mu_L}\sin^3(\lambda - \beta), \tag{6.3b}$$

$$t_3(\lambda) = \frac{d\lambda}{ds}\frac{15}{16\mu_L}\sin^5(\lambda - \beta), \tag{6.3c}$$

$$t_4(\lambda) = \frac{d\lambda}{ds}\left(\frac{3675}{8147\mu_L}\right)\left(\sin(\lambda - \beta) + \frac{1}{4}\sin 3(\lambda - \beta) + \frac{1}{10}\sin 5(\lambda - \beta) + \frac{1}{28}\sin 7(\lambda - \beta)\right), \tag{6.3d}$$

where $d\lambda/ds = (a^2 \sin^2\lambda + b^2\cos^2\lambda)^{-1/2}\,(\cos^2\phi + c^2\sin^2\phi)^{-1/2}$. The choice of $t_4(\lambda)$ is explained below. Note that each $t_q(\lambda)$ satisfies the orthogonality condition (4.15). In Table 6.3, $e = 0.866$, $\alpha = 0.87266$, $\beta = -0.54105$, $n = 32$, $\nu_1 = (\mu_4 + \mu_5)/2$ and $\nu_2 = (\mu_{22} + \mu_{23})/2$. These results are typical; dependence on the parameter values will be discussed later.

The graphs of $\mu_L t_q(\lambda)/(ds/d\lambda)$ for $q = 1,\ldots, 4$, with $\beta = 0$ are shown in Fig. 6.1. For each function the total tension applied (in each direction) is μ_L^{-1}. A peaked profile may readily be obtained with an odd power of a sine function. A flat profile may be constructed from a trigonometric polynomial of sines. The Fourier series of a square wave is unsuitable due to the Gibbs phenomenon but by taking $(C, 1)$ sums (i.e., the arithmetic means of the partial sums of the Fourier series) a satisfactory

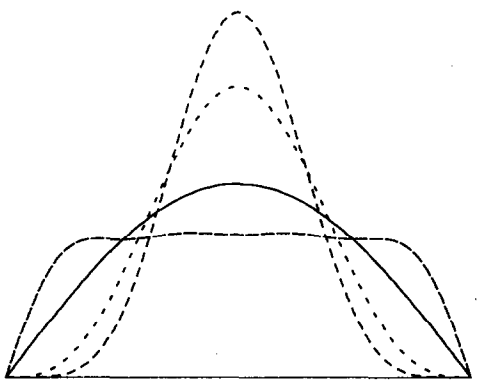

FIG. 6.1. Graphs of the traction profiles. (—, $fn = t1$; ---, $fn = t2$; – – –, $fn = t3$; and ————, $fn = t4$.)

smoothing was achieved; $t_4(\lambda)$ is the arithmetic mean of the first four partial sums of the Fourier series of a square wave.

An alternative means of obtaining a flat profile was investigated in which piecewise-constant values were smoothly joined with sections of fifth powers of sines, satisfying the orthogonality relation (4.15) while ensuring the continuity of the fifth derivative of $G(\lambda)$. The results obtained with these functions were markedly inferior to those obtained with $t_4(\lambda)$. The reason lies in the fact that $t_4(\lambda)$ is a C^∞ function and periodic. The Euler–Maclaurin sum formula predicts exponentially fast convergence in the latter case compared with $O(h^5)$ convergence for the C^5 function.

As the extra collocation points v_1 and v_2 are varied different solutions of the integral equation are obtained, but the values $F_\mu(v_i)$ should remain near zero. More importantly the different solutions should generate values of V which differ at the most by a rigid-body motion. The results which are given in the next section show that the effect of varying the points v_i is minimal.

(iv) *Calculation of the Field Variables*

The values of V may be computed at any point inside or on the ellipse from Eq. (3.1). As mentioned above several different choices of v_i were made (with otherwise identical data) to generate solutions for V. Since all such solutions differ only by a linear function of X (cf. (3.5a)), this should hold in some approximate sense for the computed solutions. By taking the difference of two such solutions a linear interpolant was constructed using two data points and the difference between the interpolated difference and the computed difference evaluated at the remaining data points. Taking $\alpha = 0.87266$, $\beta = -0.54105$, and $c = 1.0$, and defining

$$\varepsilon_L = \|(V_1 - V_2)_{\text{INTERP}} - (V_1 - V_2)_{\text{COMPUTED}}\|_\infty / \|(V_1 - V_2)_{\text{COMPUTED}}\|_\infty, \quad (6.4)$$

ε_L was calculated, for $t_1(\lambda)$ and $t_4(\lambda)$, and $e = 0.866$ and 0.968. For four pairs of points v_i, and $e = 0.968$, ε_L was close to 1.93×10^{-4} in all four cases, both for $t_1(\lambda)$ and $t_4(\lambda)$. For $e = 0.866$, $\varepsilon_L \cong 2.30 \times 10^{-4}$. There was remarkably little spread, only 1 or 2 digits in the 3rd significant figure in each set of four cases.

Once V is known on the ellipse, Eqs. (2.10) and (2.11) enable $\partial V/\partial N$ and $U'(Y)$ to be evaluated. In order to calculte the stress tensor it is necessary to evaluate the tangential derivative of V, or at least the derivative in some direction other than that of the normal. The tangential derivative was computed by evaluating the derivative of the seven point-polynomial interpolant centred on the point in question. Some loss of smoothness is inevitable with such a scheme, but the excellent accuracy of the solutions of the integral equation ensured that this did not generate any undesirable noise. If such noise had occurred, then the integral representation of V inside D could have been used, first differentiating under the integral sign and then evaluating $\partial V/\partial S$ by taking limiting values up to the boundary from the interior of the domain.

(v) *An Exact Solution*

Upon tabulating the values of the field variables it was observed that $U'(Y)$ was

constant for $t(\lambda) = t_1(\lambda)$. By virtue of Eq. (3.5b) it then follows that there is a solution of this problem for which $U'(Y) = 0$, and from Eq. (2.10) and (2.11), that a solution for V, linear in X and Y, satisfies the boundary conditions. Thus

$$V = l + mX + nY \tag{6.5}$$

with l and m arbitrary. From Eq. (2.2a) we have, in this special case,

$$\sigma_{yy} = n/c$$

Substituting (6.5) and (6.3a) into (2.10) we find, after some manipulation that

$$n = \frac{1}{2} \frac{c \cos\gamma}{(c^2 \sin^2\gamma + \cos^2\gamma)^{1/2}} \frac{\sin(\lambda_T - \beta)}{\sin(\lambda_T - \lambda_E)} \frac{1}{(a^2 \cos^2\alpha + b^2 \cos^2\alpha)^{1/2}}.$$

For $\alpha = 0.87266$, $\beta = -0.54105$, $a = 1$, $e = 0.866$, and $c = 1$ it is found that $n = 0.439198$, while using the computed values of σ_{yy} to evaluate n it was found that

$$|n_{\text{approx}} - n_{\text{exact}}| < 2.9 \times 10^{-5}.$$

Note that the numerical differentiation of the computed values of V was used to find σ_{yy} here. Note also that it is only the geometry and parameterisation of the ellipse which allows such a simple solution to exist. For any other loading profiles the manipulations are quite intractable and there is no numerical evidence for the existence of further relatively simple solutions.

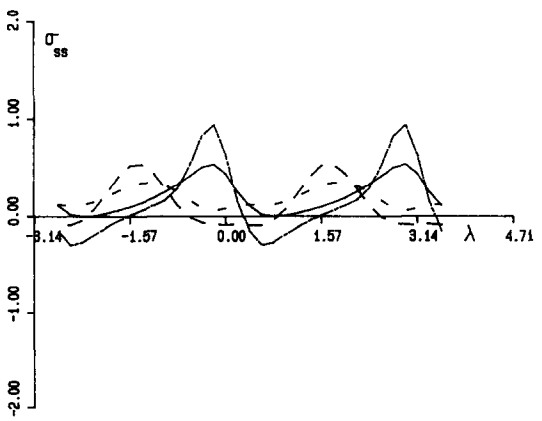

FIG. 6.2. Varying the traction profile. (—, $fn = t4$; ---, $fn = t2$; – – –, $fn = t3$; —·—, $fn = t1$; $\alpha = 0.873$; $c = 0.866$; $\beta = -0.227$; and $c = 1.0$.)

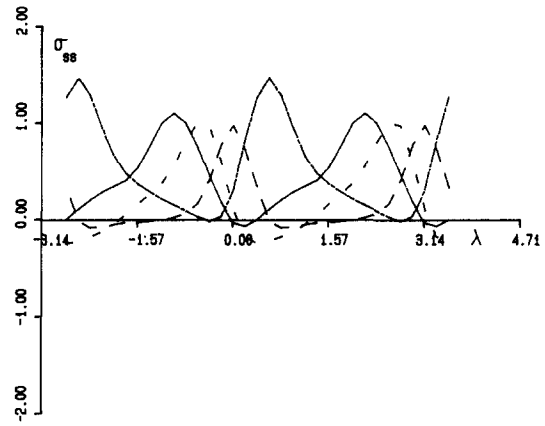

FIG. 6.3. Varying the orientation of the traction. (—, $\beta = -1.08$; – – –, $\beta = 0$; ---, $\beta = -0.537$; — — —, $\beta = 0.576$; $\alpha = 0.873$; $e = 0.866$; $c = 1.0$; and $fn = t4$.)

(vi) *General Solutions*

The graphs in Figs. 6.2–6.6 are piecewise-linear plots of the tangential stress, σ_{ss}, against the eccentric angle around the ellipse. The starting and finishing points of the curves vary because changes in parameter values alter the position of the first quadrature point. This is always situated at $\lambda = -\pi + \lambda_T$. The titles and captions explain the purpose of the plots and list the parameter values.

Figure 6.2 shows how the tangential or hoop stress changes with the traction profile, remaining tensile for the more peaked loadings and becoming compressive over about one third of the perimeter for the flattest, near-uniform load. The curve corresponding to the function t_1 may be checked by using the exact solution available in this case.

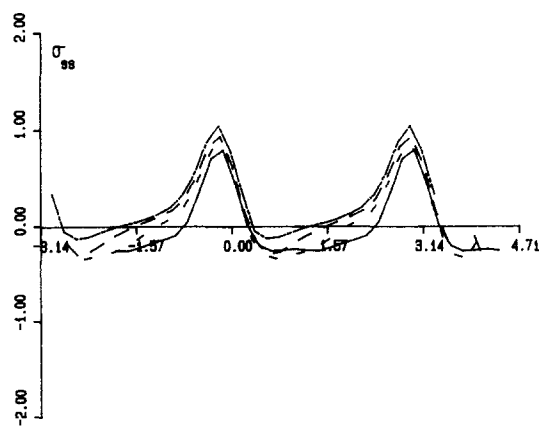

FIG. 6.4. Varying the orientation of the fibres. (—, $\alpha = 0.175$; – – –, $\alpha = 0.873$; ---, $\alpha = 0.524$; — — —, $\alpha = 1.22$; $e = 0.866$; $\beta = -0.227$; $c = 1.0$; and $fn = t4$.)

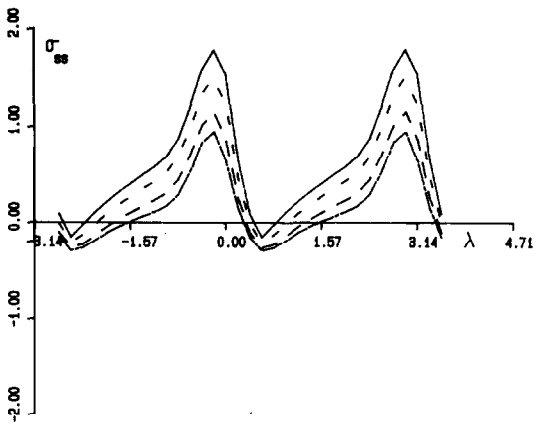

FIG. 6.5. Varying the material constant c. (—, $c = 0.5$; – – –, $c = 0.8$; ---, $c = 0.6$; —·—, $c = 1.0$; $\alpha = 0.873$, $e = 0.866$; $\beta = -0.227$; and $fn = t4$.)

Figure 6.3 shows the effect of varying the angle at which the tension is applied. The curves show that the width of the interval over which compressive values of tangential stress occur is greatest when the direction of the applied tension is nearly perpendicular to the fibre direction. As this angle is reduced the width of the interval broadens and the magnitude of the compressive values diminishes to zero.

The effect of the orientation of the fibre lines is shown in Fig. 6.4. Note that for these curves β is fixed and thus the angle between the direction of the applied traction and the fibre lines remains nearly constant. The shape of the curves remains remarkably similar, the greatest differences being the range of values over which the hoop stress is compressive.

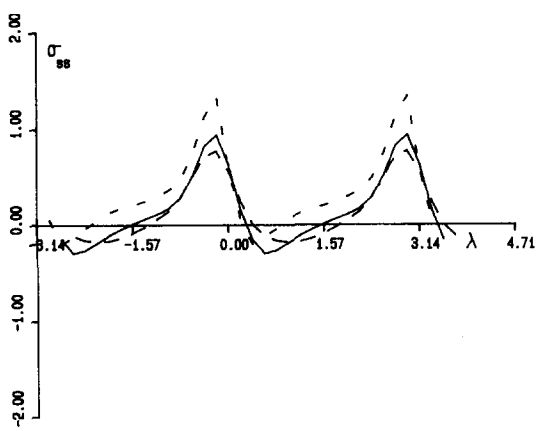

FIG. 6.6. Varying the eccentricity. (—, $e = 0.866$; – – –, $e = 0.6$; ---, $e = 0.968$; $\alpha = 0.873$; $\beta = -0.227$; $c = 1.0$; and $fn = t4$.)

The graphs in Fig. 6.5 show that the effects of varying the material constant c are primarily restricted to the magnitude of the tangential stress with a small variation in the range of compressive values.

In Fig. 6.6 as the eccentricity increases towards unity it is observed that the curvature changes more rapidly and very high slopes occur.

It is impossible to cover all possible combinations of parameter values in a few plots, but those presented are intended to convey the general trends in the solutions as the data sets are varied.

ACKNOWLEDGMENTS

Work on this problem commenced during a Sabbatical year at the University of East Anglia. The author thanks the University of East Anglia for its hospitality and generosity in providing computing facilities and the University of Queensland for its financial support.

REFERENCES

Struct. **9** (1973), 1501–1518.

3. A. H. ENGLAND, J. E. FERRIER, AND J. N. THOMAS, Plane strain and generalised plane stress problems for fibre-reinforced materials. *J. Mech. Phys. Solids* **21** (1973), 279–301.
4. L. W. MORLAND, Existence of solutions of plane traction problems for inextensible transversely isotropic solids. *J. Austr. Math. Soc. Ser. B* **19** (1975), 40–54.
5. M. JASWON AND G. SYMM, "Integral Equation Methods in Potential Theory and Elastostatics," Academic Press, New York/London, 1977.
6. K. E. ATKINSON, A survey of numerical methods for the solution of Fredholm integral equations of the second kind, SIAM, Philadelphia, 1976.
7. A. C. PIPKIN, Stress analysis for fibre-reinforced materials, *Adv. Appl. Mech.* **19** (1979), 1–51.
8. C. T. H. BAKER, The numerical treatment of integral equations, Oxford Univ. Press (Clarendon), London/New York, 1977.